Available online at www.sciencedirect.com
ScienceDirect
Trans. Nonferrous Met. Soc. China 30(2020) 2510−2517
Transactions of Nonferrous Metals Society of China
www.tnmsc.cn

Combustion synthesis of FeAl−Al_2O_3 composites with TiB_2 and TiC additions via metallothermic reduction of Fe_2O_3 and TiO_2

Chun-Liang YEH, Chih-Yao KE

Department of Aerospace and Systems Engineering, Feng Chia University, Taichung 40724, Taiwan, China

Received 14 November 2019; accepted 10 July 2020

Abstract: Combustion synthesis involving metallothermic reduction of Fe_2O_3 and TiO_2 was conducted in the mode of self-propagating high-temperature synthesis (SHS) to fabricate FeAl-based composites with dual ceramic phases, TiB_2/Al_2O_3 and TiC/Al_2O_3. The reactant mixture included thermite reagents of $0.6Fe_2O_3$+$0.6TiO_2$+2Al, and elemental Fe, Al, boron, and carbon powders. The formation of xFeAl−$0.6TiB_2$−Al_2O_3 composites with x=2.0−3.6 and yFeAl−0.6TiC−Al_2O_3 composites with y=1.8−2.75 was studied. The increase of FeAl causes a decrease in the reaction exothermicity, thus resulting in the existence of flammability limits of x=3.6 and y=2.75 for the SHS reactions. Based on combustion wave kinetics, the activation energies of E_a=97.1 and 101.1 kJ/mol are deduced for the metallothermic SHS reactions. XRD analyses confirm in situ formation of FeAl/TiB_2/Al_2O_3 and FeAl/TiC/Al_2O_3 composites. SEM micrographs exhibit that FeAl is formed with a dense polycrystalline structure, and the ceramic phases, TiB_2, TiC, and Al_2O_3, are micro-sized discrete particles. The synthesized FeAl−TiB_2−Al_2O_3 and FeAl−TiC−Al_2O_3 composites exhibit the hardness ranging from 12.8 to 16.6 GPa and fracture toughness from 7.93 to 9.84 MPa·$m^{1/2}$.

Key words: FeAl-based composites; self-propagating high-temperature synthesis; metallothermic reduction; activation energy

1 Introduction

FeAl and NiAl are important intermetallic compounds for high-temperature structural applications, due to inexpensive raw materials, high melting point, low density, good heat resistance, and excellent high-temperature oxidation and sulfidation resistance [1−4]. Because of high mechanical durability and outstanding corrosion resistance, porous FeAl alloys are considered as competitive filtration materials for efficient separation of solids and reduction of hazardous emission from hot feed gas streams [5−7]. Considerable efforts have been made to improve the mechanical strength and wear resistance of FeAl and NiAl by reinforcing intermetallics with hard ceramic compounds, such as TiB_2, TiC, TiN, WC and Al_2O_3 [8−14].

A number of fabrication methods have been utilized to produce FeAl-based composites with ceramic reinforcements, including liquid-phase sintering [8], mechanical alloying [9], pulsed current sintering [10,11], and thermal explosion [6,7,12]. Alternatively, combustion synthesis in the mode of self-propagating high-temperature synthesis (SHS) has the merits of high energy effectiveness, short reaction time, simplicity of operation, good purification capability, a diversity of products, and in situ formation of composite components [13−16]. The SHS reactions between metallic reactants (such as Ti, Al and Fe) are generally less exothermic than those between metals (e.g., Ti, Zr and Ta) and non-metals (e.g., B, C and N) [16]. Because formation enthalpies of iron aluminides are too low to synthesize FeAl and Fe_3Al through direct combustion between elemental Fe and Al, there have been few studies on the formation of FeAl-based composites by the SHS method. Lately, LIU et al [7,12] took advantage of

Corresponding author: Chun-Liang YEH; Tel: +886-4-24517250; E-mail: clyeh@fcu.edu.tw
DOI: 10.1016/S1003-6326(20)65397-3

highly-exothermic reduction of Fe_2O_3 by Al and produced FeAl−Al_2O_3 composites from thermite-containing reagents of Fe, Al and Fe_2O_3 via a thermal explosion process followed by sintering at 1100 °C for 1 h.

The objective of the present study was to investigate the fabrication of FeAl intermetallics reinforced with dual ceramic phases, TiB_2/Al_2O_3 and TiC/Al_2O_3, by means of metallothermic combustion synthesis in the SHS mode. The thermite mixture contained Al, Fe_2O_3 and TiO_2. Boron and carbon powders were added for the synthesis of TiB_2 and TiC, respectively. In this study, combustion wave dynamics, flammability limits, and activation energies of synthesis reactions were explored. The phase composition and microstructure of the as-synthesized composites as well as their hardness and fracture toughness were characterized.

2 Experimental

The starting materials of this study included Fe_2O_3 (Alfa Aesar Co., <45 μm, 99.5% purity), TiO_2 (Alfa Aesar Co., 1−2 μm, 99.5% purity), Fe (Alfa Aesar Co., <45 μm, 99.5% purity), Al (Showa Chemical Co., <45 μm, 99.9% purity), amorphous boron (Noah Technologies Corp., <1 μm, 92% purity), and carbon black (Showa Chemical Co., 20−40 nm, 99% purity). Two combustion systems were formulated as Reactions (1) and (2) for the formation of FeAl−TiB_2−Al_2O_3 and FeAl−TiC−Al_2O_3 composites:

$$0.6Fe_2O_3+0.6TiO_2+(x+2)Al+(x-1.2)Fe+1.2B \rightarrow xFeAl+0.6TiB_2+Al_2O_3 \quad (1)$$

$$0.6Fe_2O_3+0.6TiO_2+(y+2)Al+(y-1.2)Fe+0.6C \rightarrow yFeAl+0.6TiC+Al_2O_3 \quad (2)$$

where stoichiometric coefficients, x and y, signify the molar content of FeAl formed in the final products of Reactions (1) and (2), respectively. Reactions (1) and (2) adopt a thermite mixture containing Fe_2O_3 and TiO_2 as the oxidants and Al as the reductant. The molar composition of the thermite mixture is formulated under a stoichiometric proportion of $0.6Fe_2O_3+0.6TiO_2+2Al$. In addition to thermite reagents, Reaction (1) comprises extra Al (with an amount denoted by x) and elemental Fe and B powders. The ratio of additional Al to the total amount of Fe (including Fe reduced from Fe_2O_3 and elemental Fe) is kept equiatomic for the synthesis of FeAl. Besides, the molar ratio of Ti reduced from TiO_2 to elemental B in Reaction (1) is 1:2 and to carbon in Reaction (2) is 1:1 for the formation of TiB_2 and TiC, respectively. It should be noted that FeAl-based composites produced from Reactions (1) and (2) have similar contents of ceramic phases. In addition to the same quantity of Al_2O_3, the amount of TiB_2 is equivalent to that of TiC. It is recognized that Fe_2O_3 is a strong exothermic thermite oxidant, while TiO_2 is relatively weak [17]. In this study, TiO_2 plays a role in moderating the violent reaction between Fe_2O_3 and Al, and the use of TiO_2 as the source of Ti is cost-effective.

The reactant powders were dry mixed in a ball mill for 6 h and then the mixture was uniaxially pressed to cylindrical green compacts of 7 mm in diameter, 12 mm in height, and 60% of the relative density. The SHS experiments were conducted in a windowed stainless-steel chamber under a high-purity argon environment (99.99%). The combustion temperature and propagation velocity of combustion wave (V_f) were measured. Details of experimental method were reported elsewhere [18]. The synthesized composites were characterized by an X-ray diffractometer (Bruker D2) and a scanning electron microscope (Hitachi, S3000H) along with energy dispersive spectroscope (EDS). The fracture toughness (K_{IC}) of the product was determined by the indentation method using the following equation proposed by EVANS and CHARLES [19]:

$$K_{IC}=0.16H_v a^{1/2}(c/a)^{-3/2} \quad (3)$$

where H_v is the Vickers hardness, a is the half of the average length of two diagonals of the indentation, and c is the radial crack length measured from the center of the indentation. The Vickers hardness (H_v) was evaluated from the following equation considering the applied load (P) and the diagonal length d (=2a) of the indentation [20]:

$$H_v=1.8544P/d^2 \quad (4)$$

3 Results and discussion

3.1 Self-propagating combustion characteristics

Figures 1(a) and (b) illustrate time sequences of combustion images recorded from Reactions (1) and (2) under the same stoichiometric coefficient of 2.5. It is evident that a combustion wave forms

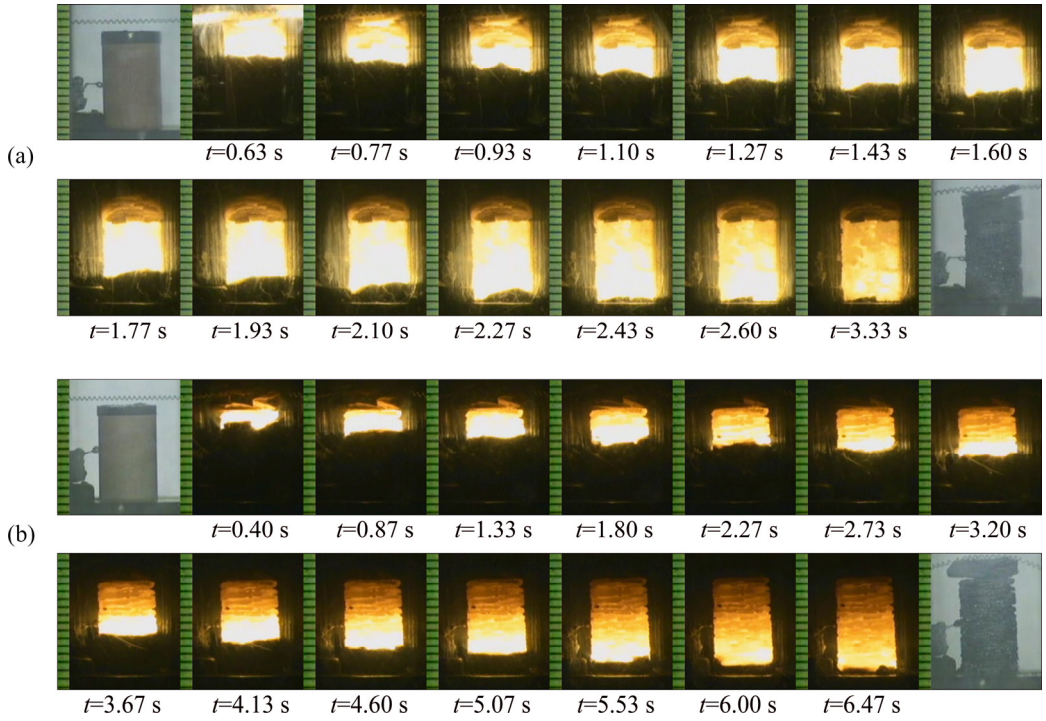

Fig. 1 Time sequences of recorded images illustrating self-propagating combustion wave of Reaction (1) with x=2.5 (a) and Reaction (2) with y=2.5 (b)

upon ignition and propagates along the sample compact in a self-sustaining manner. The flame spreading time for the combustion wave to traverse the entire sample is much shorter in Fig. 1(a) when compared with that in Fig. 1(b). This implies a higher reaction rate for Reaction (1), because possibly of greater reaction exothermicity.

The increase of Fe and Al in Reactions (1) and (2) for production of large amounts of FeAl tends to weaken the reaction exothermicity, since formation enthalpy of FeAl (ΔH_f=−50.2 kJ/mol [1]) is much lower than the heat liberated from aluminothermic reduction of metal oxides (i.e., $0.6Fe_2O_3+0.6TiO_2+2Al$ with ΔH=−614.84 kJ [21]). That is to say, elemental Fe and Al powders act as not only reactants to form FeAl but also diluents of the combustion process. As a result, the flammability limit of the SHS reaction relies on the content of FeAl to be produced. It was determined in this study that x=3.6 and y=2.75 are the flammability limits of Reactions (1) and (2), respectively. A broader combustible range for Reaction (1) was most likely attributed to a larger formation enthalpy for TiB_2 (ΔH_f=−315.9 kJ/mol) in comparison with TiC (ΔH_f=−184.1 kJ/mol) [21]. Table 1 lists the calculated overall reaction enthalpy (ΔH_r) per unit mole of the product for Reactions (1) and (2) with different stoichiometric coefficients (x and y). The value of ΔH_r decreases with increasing FeAl fraction of the final product, because mainly of the relatively low formation enthalpy of FeAl. Though the ranges of x and y are different, the reaction enthalpies for Reactions (1) and (2) shown in Table 1 are comparable. This explains different combustion ranges conducted for Reactions (1) and (2).

Experimental evidence indicated that due to considerable heat release, violent combustion and massive melting of the powder compact occurred when x was less than 2.0 for Reaction (1) and y was

Table 1 Reaction enthalpy per unit mole of product (ΔH_r) for Reactions (1) and (2)

Reaction (1)		Reaction (2)	
x	ΔH_r/(kJ·mol^{-1})	y	ΔH_r/(kJ·mol^{-1})
2.0	−251.33	1.8	−239.90
2.5	−226.80	2.0	−229.36
3.0	−207.60	2.25	−217.73
3.3	−197.97	2.5	−207.50
3.6	−189.44	2.75	−198.47

less than 1.8 for Reaction (2). This amplified the measurement uncertainty of combustion wave velocity and reaction temperature. On the contrary, it was found that under the conditions of x larger than 3.6 in Reaction (1) and y larger than 2.75 in Reaction (2), combustion failed to propagate throughout the sample and quenched halfway. This was caused largely by lack of sufficient reaction enthalpy. Consequently, the scope of experimental variables conducted by this study was set at $2.0 \leq x \leq 3.6$ for Reaction (1) and $1.8 \leq y \leq 2.75$ for Reaction (2).

Deduced flame-front propagation velocities (V_f) of Reactions (1) and (2) with respect to their stoichiometric coefficients, x and y, are presented in Fig. 2. With the increase of x from 2.0 to 3.6, Fig. 2 indicates that the combustion front velocity of Reaction (1) decreases significantly from 5.18 to 1.99 mm/s. Reaction (2) exhibits a slower combustion speed that declines from 2.62 mm/s at y=1.8 to 1.05 mm/s at y=2.75. The decrease of combustion front velocity with increasing FeAl content is caused by the low formation exothermicity of FeAl. Although the reaction between Fe and Al is an exothermic reaction, the adiabatic temperature of the Fe–Al intermetallic reaction (T_{ad}=1440 K) is less than the threshold temperature of 1800 K for the reaction to be self-sustaining. As mentioned above, the Fe−Al reaction is less energetic when compared with the reduction of Fe_2O_3 with Al and the reaction of Ti with B or C. Therefore, the increase of FeAl in the final product could lower the overall reaction exothermicity, which is most likely responsible for deceleration of the combustion wave. Moreover, becauseTiB_2 is a more exothermic phase than TiC, Reaction (1) exhibits a higher flame-front velocity than Reaction (2) when both reactions have close stoichiometric coefficients.

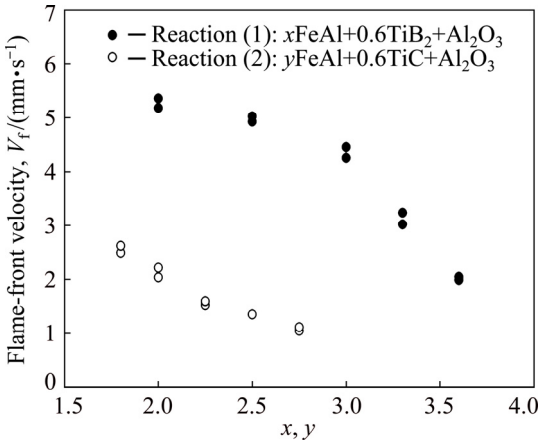

Fig. 2 Effects of FeAl content on flame-front velocity of Reactions (1) and (2) for formation of xFeAl−0.6TiB_2−Al_2O_3 and yFeAl−0.6TiC−Al_2O_3 composites

The dependence of combustion wave velocity on the reaction exothermicity was further examined by measured combustion temperatures plotted in Fig. 3. The abrupt rise in temperature signifies the rapid arrival of combustion wave and the peak value corresponds to the combustion front temperature (T_c). After the passage of combustion wave, a substantial decline in temperature stands for a rapid cooling rate due to heat loss to the surroundings. As revealed in Fig. 3, the combustion front temperatures of Reaction (1) with x=2.0 and 3.6 are 1460 and 1160 °C, respectively. This is indicative of a large decrease in the combustion exothermicity. A similar trend is observed in Reaction (2). Figure 3 shows that a peak combustion temperature of 1241 °C is detected for Reaction (2) with y=1.8 and 1066 °C is detected with y=2.5. The combustion front temperature confirms a decrease in the reaction exothermicity with increasing FeAl content formed in the composite and provides evidence of higher exothermicity for Reaction (1) than Reaction (2).

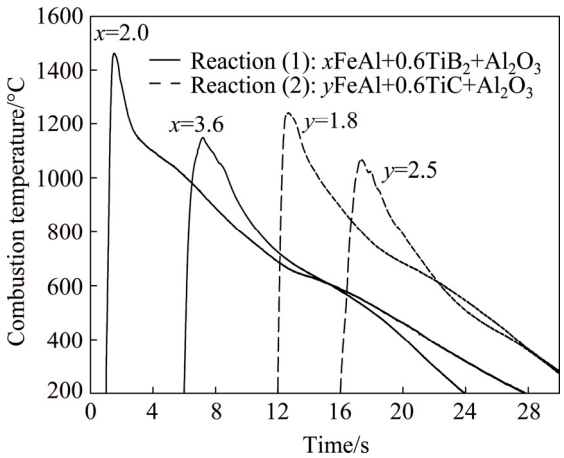

Fig. 3 Effects of FeAl content on combustion temperature of Reactions (1) and (2) for formation of xFeAl−0.6TiB_2−Al_2O_3 and yFeAl−0.6TiC−Al_2O_3 composites

The temperature dependence of combustion wave velocity offers a relationship for the determination of activation energy (E_a) of a solid-state combustion reaction. The propagation of combustion wave can be described by an energy

equation with a heat source and expressed as Eqs. (5) and (6) [22]:

$$\rho c_p V_f \frac{dT}{dx} = \frac{d}{dx}\left(\lambda \frac{dT}{dx}\right) + Q\rho\varphi(\eta,T) \quad (5)$$

$$\varphi(\eta,T) = V_f \frac{d\eta}{dx} \quad (6)$$

where Q represents the heat of reaction, c_p is the specific heat capacity, ρ is the density, φ is the reaction degree function, and η denotes the reactant conversion.

Equation (5) can be rewritten as

$$\frac{d}{dx}\left(\lambda \frac{dT}{dx}\right) - \rho c_p V_f \frac{dT}{dx} + Q\rho V_f \frac{d\eta}{dx} = 0 \quad (7)$$

Integrating Eq. (7) with the adoption of $\phi(\eta,T)=\varphi(\eta)k_0\exp[E_a/(RT)]$ yields

$$\frac{\rho V_f^2}{\lambda}\frac{d\eta}{dT} = \frac{\varphi(\eta)k_0 \exp[-E_a/(RT)]}{Q(1-\eta)} \quad (8)$$

Equation (8) can be integrated through a separation of variables to obtain Eqs. (9) and (10):

$$V_f^2 = \frac{2\lambda}{\rho Q}\frac{RT_c^2}{E_a}k_0 \exp[-E_a/(RT_c)] \quad (9)$$

$$\ln\left(\frac{V_f}{T_c}\right)^2 = -\frac{E_a}{RT_c} + \text{constant} \quad (10)$$

The formula of Eq. (10) has been widely used to determine the activation energy (E_a) from experimental data of V_f and T_c [22,23]. A plot correlating $\ln(V_f/T_c)^2$ with $1/T_c$ for Reactions (1) and (2) is depicted in Fig. 4. Based on the slopes of best-fitted linear lines, the activation energies of E_a=97.1 and 101.1 kJ/mol were deduced for Reactions (1) and (2), respectively. Because the activation energy is dependent on the reaction mechanism, two activation energies close to each other suggest that Reactions (1) and (2) should be governed by similar reaction steps. Compared to borothermic and carbothermic reduction of metal oxides, aluminothermic reduction is more favorable in both kinetic and thermodynamic aspects.

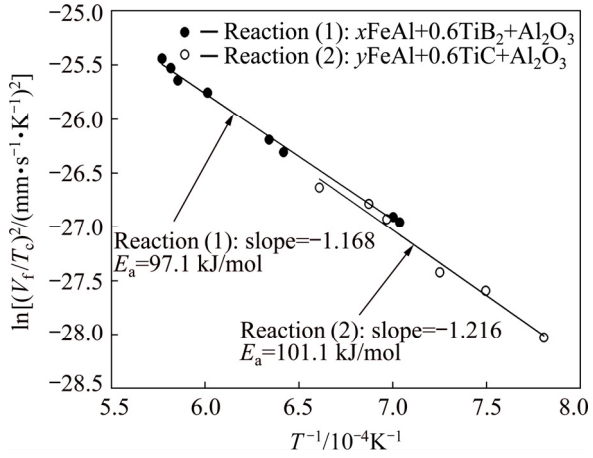

Fig. 4 Correlation of combustion front velocity (V_f) with temperature (T_c) for determination of activation energies (E_a) of Reactions (1) and (2)

The reaction mechanism of Reactions (1) and (2) can be described by a series of the reaction steps presented below. Aluminothermic reduction of Fe_2O_3 is considered as the initiation step followed by reduction of TiO_2 by Al. Two reduction reactions not only produce metal elements (Fe and Al), but also generate a substantial amount of heat to facilitate subsequent reactions. They include metal combustion between Fe and Al to form FeAl, as well as the reaction of Ti with boron in Reaction (1) to produce TiB_2 and with carbon in Reaction (2) to yield TiC:

$$Fe_2O_3+2Al \rightarrow 2Fe+Al_2O_3 \quad (11)$$

$$TiO_2+4/3Al \rightarrow Ti+2/3Al_2O_3 \quad (12)$$

$$Fe+Al \rightarrow FeAl \quad (13)$$

$$Ti+2B \rightarrow TiB_2 \quad (14)$$

$$Ti+C \rightarrow TiC \quad (15)$$

3.2 Phase composition and microstructure of FeAl-based composites

Typical XRD patterns of as-synthesized products from Reactions (1) and (2) are shown in Fig. 5. The peaks associated with FeAl, TiB_2, and Al_2O_3 are identified in Fig. 5(a). Likewise, Fig. 5(b) points out that the composite synthesized from Reaction (2) is composed of FeAl, TiC and Al_2O_3.

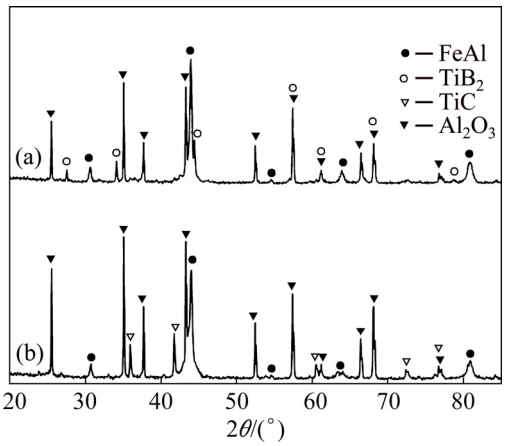

Fig. 5 XRD patterns of SHS-derived composites: (a) 3FeAl−0.6TiB_2−Al_2O_3; (b) 2.25FeAl−0.6TiC−Al_2O_3

Almost no impurities or unreacted phases are detected. This confirms complete conversion from the reactants to FeAl composites with dual ceramic phases, TiB_2/Al_2O_3 and TiC/Al_2O_3, through aluminothermic SHS reactions.

SEM micrographs shown in Figs. 6(a) and (b) presents the fracture surface of FeAl-based composites synthesized from Reactions (1) and (2), respectively. As illustrated in Figs. 6(a) and (b), the FeAl intermetallic phase is formed with a dense and polycrystalline structure. Ceramic compounds (Al_2O_3 and TiB_2 or TiC) exist as micro-sized grains and they distribute over the surface or are embedded in FeAl. It is useful to note that SHENG et al [24] fabricated a similar composite of $NiAl−TiC−Al_2O_3$ via SHS with hot extrusion and performed a detailed microstructure characterization. They reported that TiC and Al_2O_3 exhibited an obvious trend to distribute along extrusion direction. In the composite, TiC particles along NiAl grain boundary agglomerated and grew, but the TiC particles in NiAl grain were fine [24].

EDS spectra presented along with Fig. 6(a) provide the molar ratios of elements including Fe:Al=51.07:48.93, Ti:B=34.35:65.65 and Al:O=38.38:61.62. This confirms the formation of FeAl, TiB_2, and Al_2O_3 from Reaction (1). As indicated in Fig. 6(b), the molar ratios of Fe:Al=50.03:49.97 and Ti:C=50.79:49.21 obtained from EDS spectra match closely with those of FeAl and TiC, respectively, from Reaction (2).

The variations of Vickers hardness and fracture toughness with product composition are presented in Fig. 7. With the increase of the FeAl content from x=2.0 to 3.6 in Reaction (1), Fig. 7 shows that the xFeAl−0.6TiB_2−Al_2O_3 composites exhibit a decrease in Vickers hardness from 16.6 to 12.8 GPa. The increase of FeAl content in the intermetallic/ceramic composite means a decrease in the proportion of ceramic phases. This result confirms the role played by ceramic phases in improving the hardness of FeAl-based composites. As indicated also in Fig. 7, the xFeAl−0.6TiB_2−Al_2O_3 composite retains sufficient toughness with K_{IC} ranging from 7.93 to 9.84 MPa·$m^{1/2}$ for x=2.0−3.6. In summary, an intermetallic/ceramic composite composed of 3.6FeAl−0.6TiB_2−Al_2O_3 possesses the decent properties of H_v=12.8 GPa and K_{IC}=9.84 MPa·$m^{1/2}$.

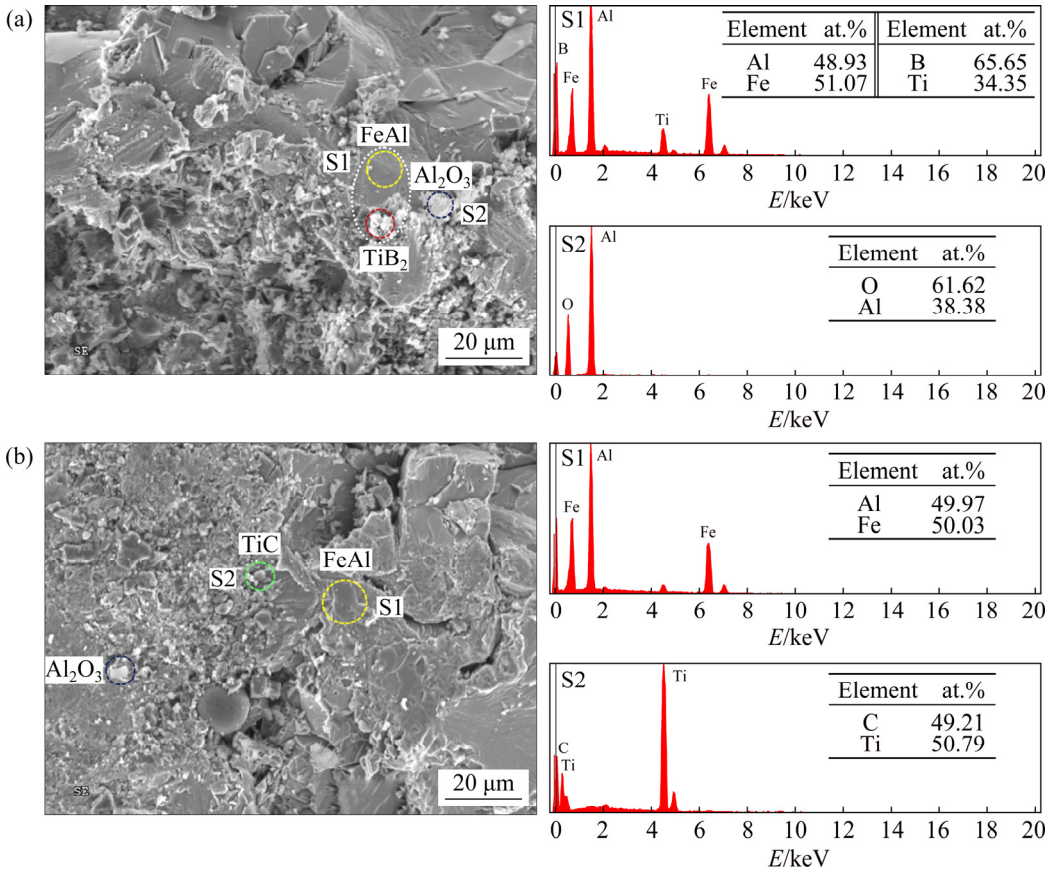

Fig. 6 SEM micrographs and EDS spectra of fracture surface of FeAl-based composites of 3FeAl−0.6TiB_2−Al_2O_3 (a) and 2.5FeAl−0.6TiC−Al_2O_3 (b)

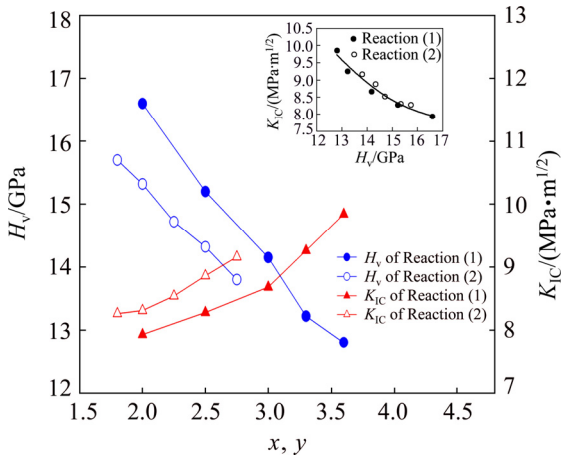

Fig. 7 Variations of Vickers hardness and fracture toughness with FeAl content of xFeAl−0.6TiB_2−Al_2O_3 (x=2.0−3.6) and yFeAl−0.6TiC−Al_2O_3 (y=1.8−2.75) composites

A similar trend to the products of Reaction (1) is observed for the yFeAl−0.6TiC−Al_2O_3 composites of Reaction (2). With y increasing from 1.8 to 2.75, Fig. 7 reveals that Vickers hardness decreases from 15.7 to 13.8 GPa and K_{IC} increases from 8.26 to 9.16 MPa·m$^{1/2}$. The insert of Fig. 7 presents the relationship between Vickers hardness and fracture toughness of TiB_2/Al_2O_3- and TiC/Al_2O_3-added FeAl composites, which is in good agreement with that of the WC−FeAl composite [25].

4 Conclusions

(1) Experimental evidence shows that boron-containing SHS reactions are more exothermic than those involving carbon powders. The increase of FeAl reduces the reaction exothermicity and decreases the combustion wave velocity.

(2) Flammability limits of x=3.6 and y=2.75 are observed for aluminothermic SHS reactions to fabricate xFeAl−0.6TiB_2−Al_2O_3 and yFeAl−0.6TiC−Al_2O_3 composites.

(3) The XRD analysis indicates that complete phase conversion from the reactants to TiB_2/Al_2O_3- and TiC/Al_2O_3-added FeAl composites with almost no impurities.

(4) The microstructure of FeAl-based composites features a dense polycrystalline FeAl matrix with micro-sized ceramic particles scattering over its surface.

(5) Ceramic phases, TiB_2/Al_2O_3 and TiC/Al_2O_3, increase the hardness of FeAl composites with the values from 12.8 to 16.6 GPa. Maximum fracture toughness values of the TiB_2/Al_2O_3- and TiC/Al_2O_3-added FeAl composites are 9.84 and 9.16 MPa·m$^{1/2}$, respectively.

Acknowledgments

The authors are grateful for the research grant of MOST 108-2221-E-035-026 funded by the Ministry of Science and Technology.

References

[1] DEEVI S C, SIKKA V K. Nickel and iron aluminides: An overview on properties, processing, and applications [J]. Intermetallics, 1996, 4: 357−375.

[2] MASMOUDI M, MHADHBI M, ESCODA L, SUÑOL J J, KHITOUNI M. Microstructural evolution and corrosion behavior of nanocrystalline FeAl synthesized by mechanical alloying [J]. Journal of Alloys and Compounds, 2016, 657: 330−335.

[3] LIU W J, WANG Y, GE H B, LI L, DING Y, MENG L G, ZHANG X G. Microstructure evolution and corrosion behavior of Fe−Al-based intermetallic aluminide coatings under acidic condition [J]. Transactions of Nonferrous Metals Society of China, 2018, 28: 2028−2043.

[4] YILDIRIM M, AKDENIZ M, MEKHRABOV A O. Effect of Mo addition on microstructure, ordering, and room-temperature mechanical properties of Fe−50Al [J]. Transactions of Nonferrous Metals Society of China, 2018, 28: 1970−1979.

[5] ZHANG H B, LIU X L, JIANG Y, GAO L, YU L P, LIN N, HE Y H, LIU C T. Direct separation of arsenic and antimony oxides by high-temperature filtration with porous FeAl intermetallic [J]. Journal of Hazardous Materials, 2017, 338: 364−371.

[6] CAI X P, LIU Y N, FENG P Z, JIAO X Y, ZHANG L Q, WANG J Z. Fe−Al intermetallic foam with porosity above 60% prepared by thermal explosion [J]. Journal of Alloys and Compounds, 2018, 732: 443−447.

[7] LIU Y N, SUN Z, CAI X P, JIAO X Y, FENG P Z. Fabrication of porous FeAl-based intermetallics via thermal explosion [J]. Transactions of Nonferrous Metals Society of China, 2018, 28: 1141−1148.

[8] SCHNEIBEL J H, CARMICHAEL C A, SPECHT E D, SUBRAMANIAN R. Liquid-phase sintered iron aluminide−ceramic composites [J]. Intermetallics, 1997, 5: 61−67.

[9] KRASNOWSKI M, KULIK T. Nanocrystalline FeAl matrix composites reinforced with TiC obtained by hot-pressing consolidation of mechanically alloyed powders [J]. Intermetallics, 2007, 15: 1377−1383.

[10] SHON I J, LEE S J. Rapid consolidation of nanostructured WC−$FeAl_3$ by pulsed current activated heating and its mechanical properties [J]. International Journal of Refractory Metals and Hard Materials, 2017, 65: 69−75.

[11] FURUSHIMA R, HYUGA H. Fabrication of dense Al_2O_3−FeAl composites by using solid-state sintering [J]. International Journal of Refractory Metals and Hard Materials, 2019, 80: 292−298.
[12] LIU Y N, CAI X P, SUN Z, JIAO X Y, AKHTAR F, WANG J Z, FENG P Z. A novel fabrication strategy for highly porous FeAl/Al_2O_3 composite by thermal explosion in vacuum [J]. Vacuum, 2018, 149: 225−230.
[13] CUI H Z, MA L, CAO L L, TENG F L, CUI N. Effect of NiAl content on phases and microstructures of TiC−TiB_2−NiAl composites fabricated by reaction synthesis [J]. Transactions of Nonferrous Metals Society of China, 2014, 24: 346−353.
[14] SONG X J, CUI H Z, CAO L L, GULYAEV P Y. Microstructure and evolution of (TiB_2+Al_2O_3)/NiAl composites prepared by self-propagation high-temperature synthesis [J]. Transactions of Nonferrous Metals Society of China, 2016, 26: 1878−1884.
[15] LIU G H, LI J T, CHEN K X. Combustion synthesis of refractory and hard materials: A review [J]. International Journal of Refractory Metals and Hard Materials, 2013, 39: 90−102.
[16] MERZHANOV A G. Combustion and explosion processes in physical chemistry and technology of inorganic materials [J]. Russian Chemical Reviews, 2003, 72: 289−310.
[17] WANG L L, MUNIR Z A, MAXIMOV Y M. Thermite reactions: Their utilization in the synthesis and processing of materials [J]. Journal of Materials Science, 1993, 28: 3693−3708.
[18] YEH C L, SUNG W Y. Combustion synthesis of Ni_3Al intermetallic compound in self-propagating mode [J]. Journal of Alloys and Compounds, 2004, 384: 181−191.
[19] EVANS A G, CHARLES E A. Fracture toughness determinations by indentation [J]. Journal of the American Ceramic Society, 1976, 59: 371−372.
[20] RIOS C T, COELHO A A, BATISTA W W, GONÇALVES M C, CARAM R. ISE and fracture toughness evaluation by Vickers hardness testing of an Al_3Nb−Nb_2Al−AlNbNi in situ composite [J]. Journal of Alloys and Compounds, 2009, 472: 65−70.
[21] BINNEWIES M, MILKE E. Thermochemical data of elements and compounds [M]. Weinheim, New York: Wiley-VCH Verlag GmbH, 2002.
[22] VARMA A, ROGACHEV A S, MUKASYAN A S, HWANG S. Combustion synthesis of advanced materials: Principals and applications [J]. Advances in Chemical Engineering, 1998, 24: 79−225.
[23] YEH C L, WANG H J. A comparative study on combustion synthesis of Ta−B compounds [J]. Ceramics International, 2011, 37: 1569−1573.
[24] SHENG L Y, YANG F, GUO J T, XI T F, YE H Q. Investigation on NiAl−TiC−Al_2O_3 composite prepared by self-propagation high temperature synthesis with hot extrusion [J]. Composites: Part B, 2013, 45: 785−791.
[25] FURUSHIMA R, KATOU K, NAKAO S, SUN Z M, SHIMOJIMA K, HOSOKAWA H, MATSUMOTO A. Relationship between hardness and fracture toughness in WC−FeAl composites fabricated by pulse current sintering technique [J]. International Journal of Refractory Metals and Hard Materials, 2014, 42: 42−46.

应用 Fe_2O_3 和 TiO_2 金属热还原进行添加 TiB_2 和 TiC 的 FeAl/Al_2O_3 复合材料的燃烧合成

叶俊良，柯智耀

逢甲大学 航太与系统工程学系，台中市 40724，台湾，中国

摘　要：通过 Fe_2O_3 和 TiO_2 金属热还原自蔓延高温合成(SHS)制备添加 TiB_2/Al_2O_3 and TiC/Al_2O_3 陶瓷相的铁铝基金属(FeAl)复合材料。反应物粉末包括铝热剂 0.6Fe_2O_3+0.6TiO_2+2Al 以及元素铁、铝、硼与炭黑。复合材料成分为 xFeAl−0.6TiB_2−Al_2O_3 (x =2.0~3.6)和 yFeAl−0.6TiC−Al_2O_3 (y =1.8~2.75)。当复合材料中 FeAl 含量增加时，燃烧反应的放热量下降，最终两组燃烧反应的可燃极限分别为 x=3.6 和 y=2.75。根据燃烧波的动力学分析，合成两种 FeAl 复合材料的反应活化能为 E_a=97.1 and 101.1 kJ/mol。从产物的 XRD 分析可确认生成 FeAl/TiB_2/Al_2O_3 和 FeAl/TiC/Al_2O_3 复合材料。SEM 显示 FeAl 为致密多晶结构，而陶瓷成分 TiB_2、TiC 和 Al_2O_3 呈微米颗粒状分散于复合材料中。合成的 FeAl−TiB_2−Al_2O_3 和 FeAl−TiC−Al_2O_3 复合材料的硬度为 12.8~16.6 GPa，断裂韧性为 7.93~9.84 MPa·$m^{1/2}$。

关键词：铁铝基金属复合材料；自蔓延高温合成；金属热还原；反应活化能

(Edited by Bing YANG)